Available online at www.sciencedirect.com

jmr&t Journal of Materials Research and Technology

www.jmrt.com.br

Original Article

High-pressure grinding rolls: model validation and function parameters dependency on process conditions

*Hernan Anticoi**, *Eduard Guasch*, *Josep Oliva*, *Pura Alfonso*, *Marc Bascompta*, *Lluis Sanmiquel*

Departament d'Enginyeria Minera, Industrial i TIC, Universitat Politècnica de Catalunya Barcelona Tech, Av. Bases de Manresa 61-73, Manresa, Barcelona, 08242, Spain

ARTICLE INFO

Article history:
Received 29 January 2019
Accepted 4 September 2019
Available online 8 October 2019

Keywords:
HPGR
Modelling
Breakage
Comminution

ABSTRACT

A model for High Pressure Grinding Rolls (HPGR) was developed in this work based on the widely used Population Balance Model (PBM). This approach uses a variety of different functions one of which is the breakage distribution function. The methodology to determine the function parameters is presented and using these values, the model was compared with real processed materials from an HPGR pilot plant, with tungsten ore as the test material. The results of the model parameter determination, and the product of the comminution in the HPGR, showed the dependency of material breakage on the material characteristics, and on the operative and process conditions. The model presented is reasonably robust, showing less error than the 3.0 Root Mean Square Error when compared with a heterogeneous feed particle size distribution material. The operational gap was also studied, and its dependency on the feed particle size, porosity, moisture, and specific pressing force was proven.

1. Introduction

The European community has been making efforts in recent years to decrease dependency on external sources of raw materials, and therefore has been encouraging the internal production of so-called strategic metals. These are metals that, due to various factors such as the risk in their supply and their importance in industry, have strategic significance [1]. One of the ways to reduce the risk of supply is to open more mines, which is sometimes possible only with optimised mineral processing methods. In terms of energy consumption, reduction in the size of the material being processed is the task that generates the greatest economic expense within a processing plant [2–4]. Understanding the mechanical behaviour of the material and the consequent prediction of the results of a grinding stage, as well as the choice of the right equipment to perform it, are key points to achieve improvement in the process. High-Pressure Grinding Roll (HPGR) stands out as one of the most efficient types of grinding machinery, in terms of energy consumption and the size reduction rate [5].

* *Corresponding author.*
E-mail: hernan.anticoi@upc.edu (H. Anticoi).

https://doi.org/10.1016/j.jmrt.2019.09.016

The prediction of the particle size distribution resulting from comminution in an HPGR device can be estimated using the Population Balance Model (PBM). This mathematical approach is decomposed into different sub-functions that describe the behaviour of the particles being processed in a high-pressure environment. First of all, there is a selection function that shows the selected particles that will be broken, and discriminates which particles have the probability of being comminuted under a single particle compression, as well as the undersized particles that will be broken by the bed particle compression effect [6–10]. In addition to this selection criterion, the nature of the distribution of the particles that have been ground is described by the breakage distribution function, B. This function indicates the progeny particle arrangement caused by comminution of every single particle from a feed population [11,12]. These mathematical expressions are structured in such a way as to depend on the feed particle size, the size reduction ratio between the parent particles and their progeny, and especially on certain parameters that are linked to the nature of the material being ground and the type of comminution equipment [13]. However, in most cases, these parameters are fitted with experimental data using a genetic algorithm, or the so-called reverse simulation or back-calculation [10,14].

The original form of the breakage distribution function was presented by Austin and Luckie [15], and its parameters have been experimentally determined in high pressure conditions by means of the piston die procedure [16]. It was demonstrated that the differences in the parameter values are related to the condition of breakage in which the test was carried out, and on their mineral composition. In this case, two breakage mechanisms have been identified and tested: the single particle compression, and the bed particle compression. This means that the breakage distribution function is non-normalisable when the nature of breakage changes. Consistent with this statement, early research on milling model parameters showed the non-normalised breakage distribution function B, specifically for brittle material [17,18]. Furthermore, in order to obtain parameter values with confidence, not only is the quality of the experimental data fundamental, but also the accuracy of the test execution. This is because in the non-normalisation of the function B, the parameter values are also given for different particle size intervals, and although they show similar behaviour, the displacement among the curves for different narrow size ranges is evident [15,17,19].

In trying to explain the nature of the breakage distribution function, some authors suggest that this function depends only on the mineral characteristics of the tested material [11,20]. In the case of the HPGR, some studies show how the energy necessary to break the particle is useful to find the breakage function parameters [21]. However, the piston die methodology showed how the mechanism of the breakage not only affects the function parameters but also has an impact on the model itself. Based on these observations, an improved Austin model [6], which is able to describe and predict the particle size distribution of HPGR, was presented [22]. Thus, this model is based on the non-normalisable breakage function parameter when the simulation runs under a single particle compression and bed particle compression conditions.

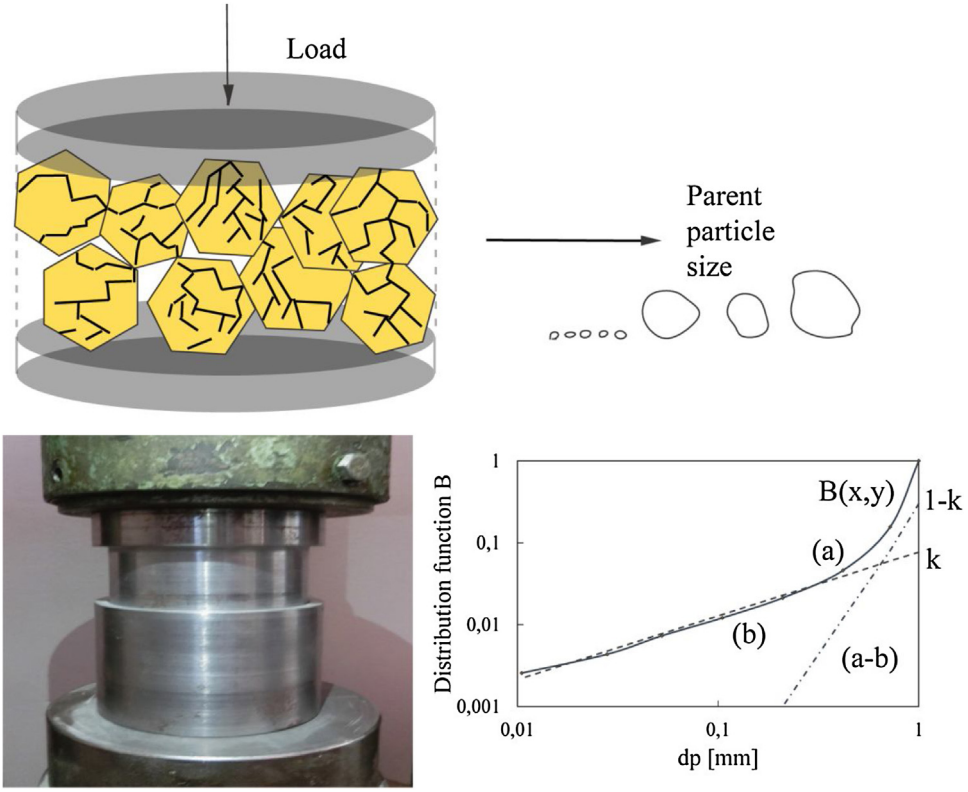

Fig. 1 – Piston-die test performed under bed compression conditions. The piston runs under a hydraulic pressure system, for different specific pressing force. The resulting particles are used to find the breakage function parameters.

Despite these new finding, other patterns could influence the values of the breakage distribution function, mainly because the mechanism of rupture could vary according to the type of operative condition in which comminution is carried out. Attrition, shear, and abrasion are predominant in ball, rod, and SAG mills [23]. However, compression in the pre-crusher stage of a single particle compression [8–10], mainly with multiple contact points [24,25], is predominant in HPGR. Moreover, the wide range of specific pressing forces under which HPGR works, have a great influence on the breakage behaviour. In the single particle compression mode, it could generate internal fractures or the collapse of the grain structure. As a single particle compression needs only two contact points to generate comminution, the daughter particles generated tend to be more homogeneous in size. Meanwhile, in bed compression, multiple contact points generate more shear and abrasion, causing the daughter particles to be heterogeneous in their size distribution [16].

The impacts of the operative parameters and material properties on the model functions have been studied. The breakage distribution function was found to be non-normalisable under different fracture mechanisms, such as in single particle compression and bed particle compression. The behaviour of this function when varying the specific pressing force was also analysed. The influence of some of the material properties such as moisture, top feed size, and porosity has also been studied. In terms of the operative set-up of the process, the specific pressing force and the roll speed have been compared with the operational working gap.

2. Methodology

2.1. Materials

The model presented previously was tested using two types of materials; a tantalum ore, which is mainly made up of altered granite obtained from ancient tin exploitation, and a tungsten ore, which is a calc-silicate scheelita ore from an underground mine [16,22]. The present study validates the current model with a third material, which is also a tungsten ore, but in this case, it is granite from the former processing plant tailings of an ancient mine in the west of Spain [26]. The main ore is scheelita, with a minor content of wolframite. This material has been used for two specific purposes: to obtain the model function parameters by means of the piston-die press methodology, and to perform pilot plant test-work.

2.2. Piston press test

The breakage function distribution parametrisation was performed at the mineral processing laboratory in the Universitat Politècnica de Catalunya (UPC) in Spain. The two predominant comminution conditions in HPGR were taken into account: bed particle compression and single particle compression. The piston-die test tries to capture these conditions in order to obtain the breakage function variables. The material intended for this purpose was sieved and classified into mono-size particles, in order to find normalisation of the breakage distribution function for different size ranges and under different operative conditions (Table 1). Based on the lab-test work, in which the HPGR was set-up with a specific pressing force Fsp of 2.5 N/mm^2, 3.5 N/mm^2 and 4.7 N/mm^2, bed compression tests were performed with the same specific pressing force values. The single particle compression tests were undertaken in only one size range, since the test on the HPGR showed that single particle compression occurs only in large-size particles, and the probability of a single compression occurring for this material is very low.

Table 1 – Sample weight (g) used for all piston-die tests.

Mesh size (mm)	Fsp (N/mm^2)			Single compression
	2.5	3.5	4.7	
−4.0 + 3.2	141.4	141.1	138.4	–
−6.3 + 4.0	171.9	173.1	162.2	–
−8.0 + 6.3	168.1	174.5	162.9	–
−9.5 + 8.0	151.5	148.7	150.8	–
−12.5 + 9.5	159.8	179.0	162.8	–
−14.0 + 12.5	165.2	164.8	152.6	211.2

The samples were compressed using a hydraulic piston-die that runs in a load range of 0–12 tonnes (equivalent to the previously mentioned specific pressing force). The force was applied on a 60 mm piston diameter (Fig. 1). For the single compression test, the particles were placed under pressure at two or fewer contact points between the surfaces of the piston, particle by particle. For the bed particle compression tests, a set of mono-size particles were confined in the piston chamber, with several inter-contact points between the particles and the piston surface.

The comminuted material was sieved and the cumulative particle size distribution was plotted against the relative size reduction ratio dp_i/dp_j, where dp_i is the progeny particle and dp_j is the parent particle. The plotted points were normalised in order to determine the breakage function parameters using Eqs. (1) and (2) [19].

$$B_{ij} = k\left(\frac{dp_i}{dp_j}\right)^{n_1} + (1-k)\left(\frac{dp_i}{dp_j}\right)^{n_2} \quad \text{for } dp_i \geq y_0 \tag{1}$$

$$B_{ij} = k\left(\frac{dp_i}{Y_0}\right)^{n_3}\left(\frac{dp_i}{dp_j}\right)^{n_1} + (1-k)\left(\frac{dp_i}{dp_j}\right)^{n_2} \quad \text{for } dp_i < y_0 \tag{2}$$

Eq. (1) is the most common one to characterise the breakage distribution function. In this case, k, n_1 and n_2 are the function parameters. When the breakage distribution function becomes bimodal, Eq. 1 and Eq. 2 are used simultaneously. Thus, the parameters are k, n_1, n_2, n_3 and Y_0, which is the largest chip size (which must be smaller than the parent size dp_j). It usually takes values of 0.05 m to achieve the ball mill breakage function [19]. For calculation purposes, the cumulative form B_{ij} is transformed into the differential from b_{ij} (Eq. 3).

$$b_{ij} = B_{i,j} - B_{i-1,j} \tag{3}$$

The model calculation and reverse adjustment were completed using Mat-lab® codes. Several optimisation algorithms were used to find the best fitted parameters with the experi-

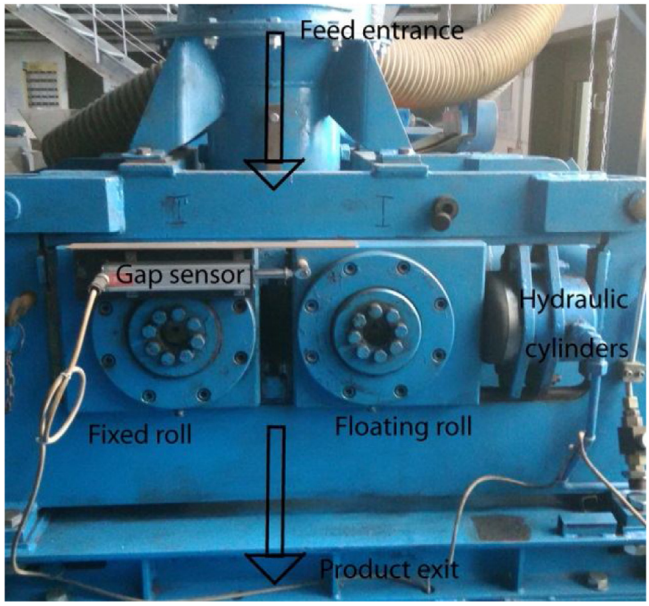

Fig. 2 – Köppern manufacturer HPGR features.

Table 2 – Specifications of the HPGR device.

	Laboratory scale HPGR	Pilot plant scale HPGR
Roll diameter	300 mm	1000 mm
Roll width	70 mm	230 mm
Rotational speed	0–0.134 m/s	0–1 m/s
Specific pressing force	0–1.307 N/mm^2	0–4.7 N/mm^2
Specific power draw	1.2–1.4 kW h/t	1.2–2.1 kW h/t

mental data. Finally, the simulation and results demonstration are shown as a validation of the new findings in particle size distribution determination.

2.3. *HPGR validation test*

The validation test work was carried out at the Köppern Aufbereitungstechnik GmbH & Co.KG pilot plant, located at the Technische Universität Bergakademie Freiberg facilities, Germany.

The machinery used for model validation consists of two robust devices. The first is an industrial type of machinery, of 1 m diameter with 0.23 m wide rolls (Fig. 2). The other is a lab-scale type of the same machinery, and has a diameter of 0.03 m and 0.07 m wide rolls. Both models have studded liners for the roller surface, and use four eccentrically nitrogen fed pistons, applying a range of pressure from 56 to 102 bar (Table 2). A set of 28 experiments were designed under different operating conditions in order to check the performance and effect of these conditions on the HPGR product (Table 3). The material was quartered and classified into different feed size ranges, from category I to category VI. The categories I to IV represents narrow particle size ranges; the V group is a heterogeneous particle size distribution. The VI group is a material used in the laboratory scale HPGR type.

2.4. *HPGR modelling*

The improved Austin model [23] has been used as a vertebral structure in this work, including the new findings on the breakage function behaviour. For this model, the single particle compression and bed compression phases are run simultaneously. For bed particles compression, two breakage functions are discriminated: one simulates the fine particles comminution and the other the coarse particles comminution. The block model highlights the bed compression stage, and shows the other sub-processes in HPGR (Fig. 3).

In the Fig. 3, the feed fi enters into the pre-crushing zone; the particles that are discriminated by the selection function over a certain size go to the single compression, and the others to the bed compression. The product f_i' is the sum of the results of both sub-processes. The selection function S_n used in this case [27], is mainly used for cone crushers, but is also applied for high-pressure grinding rolls (Eq. 4). This selection approach describes the physical process in the steps where the single particle compression occurs. This function has the particularity of fixing the upper and under edges, related to the device geometry and the mineral characteristics.

$$\begin{aligned} S_n &= 1 - \left(\frac{dp_i - x_n}{d_1 - x_n}\right)^{\gamma} && \text{for } d_1 < dp < x_n \\ S_n &= 0 && \text{for } dp < d_1 \\ S_n &= 1 && \text{for } dp > x_n \end{aligned} \tag{4}$$

In Eq. 4 x_n represents the upper limit of the function, and is given by the distance between the rolls when the nipping action begins. The parameter d_1 represents the under limit where the particles cannot be under comminution in the single compression condition due to their size. They, thus form the bed compression zone, interacting with both larger and same size particles. The parameter γ is related to the mineral characteristics and describes the behaviour of the selection function curve. The parameter x_n (Eq. 5) is a relation among all geometric characteristics of the device, material feed size, and other features as material density, the gap and the nip angle (Eq. 6) [10].

$$x_n(\alpha_n) = S_0 + D(1 - \cos(\alpha_n)) \tag{5}$$

$$\cos(\alpha_{nip}) = \frac{1}{D}\left[(S_0 + D) + \sqrt{(S_0 + D)^2 - \frac{4S_0\delta D}{\rho_a}}\right] \tag{6}$$

In Eq. 6 ρ_a is the bulk density at the feed zone, δ is the bulk density at the extrusion zone, L is the roll length, U is the tangential velocity, D is the roll diameter, and S_0 is the gap. The values of the vector S_n depend on x_n, which is a function of the angle α. If N_t is denominated as the number of single compression stages necessary to break the material until almost all particles reach the gap size and can leave the comminution zone (Fig. 4), the angles to evaluate the function x_n are defined in Eq. 7.

$$\alpha_n = \frac{N_t - (n-1)}{N_t}\alpha_{nip} \quad n = 1.\ldots.N_t \tag{7}$$

Table 3 – Material characteristics and process conditions of all tests performed in an HPGR. Fsp represents the specific pressing force, and V is the roll speed.

Category	Test number	Feed size range [mm]	Fsp [N/mm^2]	V [m/s]	Working gap [mm]	Specific work kWh/t
	1			0.56	18.0	1.2
	2		2.5	0.78	18.4	1.2
I	3	0–3		1.0	18.8	1.3
	4		3.5	0.56	16.9	1.6
	5		4.7		16.2	2.0
	6			0.56	18.5	1.1
	7		2.5	0.78	18.8	1.2
II	8	3–8		1.0	19.0	1.2
	9		3.5	0.56	17.0	1.7
	10		4.6		16.2	2.0
	11			0.56	19.8	1.2
	12		2.5	0.78	20.0	1.2
III	13	8–14		1.0	19.7	1.2
	14		3.5	0.56	17.8	1.7
	15		4.5		17.3	1.9
	16			0.56	19.8	1.5
	17		2.5	0.78	19.6	1.3
IV	18	14–22		1.0	18.8	1.4
	19		3.5	0.56	18.5	1.7
	20		4.5		17.5	2.1
	21			0.56	26.4	1.1
	22		2.6	0.78	25.4	1.1
V	23	0–22		1.0	25.5	1.1
	24		3.5	0.56	23.8	1.5
	25		4.5		23.0	1.7
	26	0–3	2.5	0.17	5.80	1.2
VI	27	3–8	2.5	0.17	6.70	1.4
	28	0–8	2.5	0.17	7.50	1.2

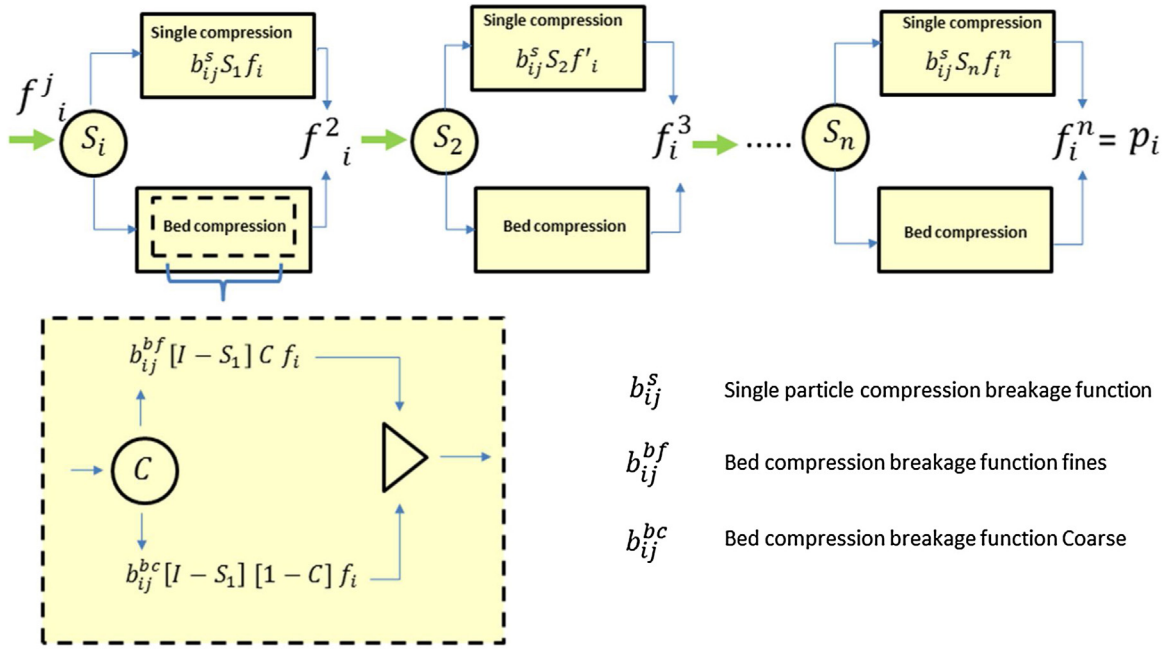

Fig. 3 – Block scheme of the improved model to predicate the HPGR particle size distribution product.

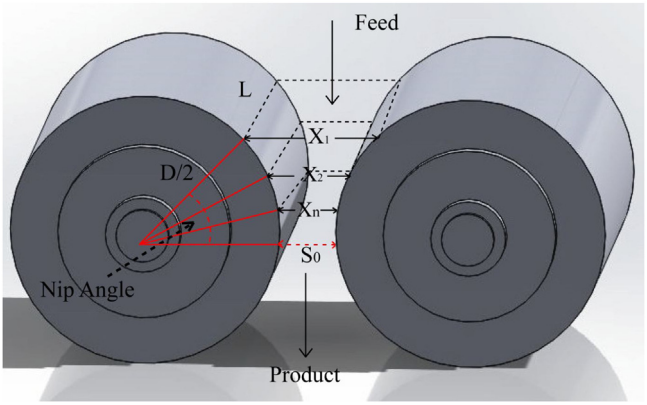

Fig. 4 – Calculation methodology for the x_n parameter which is useful for the selection function.

The bulk density of the material is also a key parameter for the model. It was measured at the inlet and outlet by means of the quotient of mass m and total volume of a sample V_B (Eq. 8).

$$\rho = \frac{m}{V_B} \tag{8}$$

In Eq. 8, the density of the feed is ρ and the product density is δ. The sample moisture was determined by weighing the initial and the final mass after drying in an oven until a constant mass was reached. Porosity (Po) is the relative relation between material density and bulk density (Eq. 9).

The model fit was evaluated using the Root Mean Square Error (RMSE), which measures the agreement between the experimental data and the model predictions (Eq. 10).

$$Po = \left(\frac{\rho_i - \rho_b}{\rho_i}\right) \tag{9}$$

$$RMSE = \sqrt{\frac{1}{N}\sum_{i=1}^{N}(p_i - y_i)^2} \tag{10}$$

In Eq. 10, the parameter N is the length of the input vector, p_i is the experimental values of the vector and y_i represents the simulated values.

The percentage variation between the calculated and experimental values (Eq. 11) has been also used to evaluate local differences in the model simulation.

In Eq. (11), V_i is the experimental value and V_f is the final model predicted value.

$$\% = 100\,x\,\frac{|V_i - V_f|}{|V_i|} \tag{11}$$

3. Results and discussion

3.1. *Breakage distribution function*

The piston–die test results are presented in their standardised form: the cumulative percentage mass is plotted against the particle size reduction dpi/dpj ratio. In order to observe the variations of the curves for different operative conditions, each test was grouped by a narrow size range (Fig. 5), and are also presented according to the specific pressing force (Fsp) used: 2.5 N/mm^2, 3.5 N/mm^2 or 4.7 N/mm^2 (Fig. 6). All narrow size range categories show the same patterns, slopes, and curvature. In the test with −4 + 3.15 mm size range (Fig. 5A), the displacement of the curves when the Fsp changes is clear and conclusive; the breakage function distribution has to have different parameters with variations in the Fsp. The other tests confirm this finding (Fig. 5B–F). Since the variation of the cumulative mass seems to be similar, except for the −14 + 12.5 mm size range, it is necessary to observe the patterns when the curves are grouped based on Fsp values. Fig. 6B–D shows all the narrow size test results for each Fsp. Initially, the results appear dispersed. However, two categories of curves can be distinguished for the higher specific pressing forces of Fsp (Fig. 6C and D); that is, for 3.5 N/mm^2 and 4.7 N/mm^2. Three categories can be distinguished for lower specific pressing forces (2.5 N/mm^2, Fig. 6B). Therefore, these observations of the results have been used to identify different sub-phases in the back-calculation procedure of the parameters of the breakage distribution function. In summary, for Fsp 2.5 N/mm^2, the particles between 3.0 mm and 8 mm are categorised as fine phase particles, those between 8.0–12.5 mm are considered in the medium size range, and a narrow range between 12.5 and 14.0 mm represents the top-size. In the case of the Fsp values of 3.5 N/mm^2 and 4.7 N/mm^2, the categories are fine phase particles between 3.0 mm and 8 mm, and medium size particles between 8.0 mm and 14.0 mm (Table 4).

Thus, using Eq. 1 and values from Table 4, the resulting breakage distribution function is presented for all tested specific pressing forces (Fsp) and size ranges (Fig. 7) and for the single particle compression condition. The particle size distribution model presented in this study has been modified in order to introduce this new finding regarding the breakage distribution function.

3.2. *Model validation*

The results of all sieve analyse from this work are presented in Fig. 8. They are grouped into six feed size categories (from group I to group V in the case of large HPGR and the group VI, tests performed with the lab-scale device). The feed particle size distribution should be similar for each category, except the group V, which represents a heterogeneous size distribution (Fig. 8A). The feed and product PSD of the material used with the laboratory scale HPGR are also presented (Fig. 8B and D).

The results of the comminution product of all tests in the large HPGR (Fig. 8C) show that some patterns depended on the feed size in categories I and II. However, the plotted lines overlap from categories III to V. If the behaviour of the product is carefully observed, it is possible to compare the differences in the generation of particle sizes when the pressure conditions change. The curves of category II, from tests 6 to 10 were zoomed (Fig. 9). The first types of curves are generated, when the roll speed is varied. Although there is a distance between these curves, these are not as evident as the distances between curves with different specific pressing forces. This fact reaffirms the usage of different breakage distribution function parameters when the specific pressing force varies.

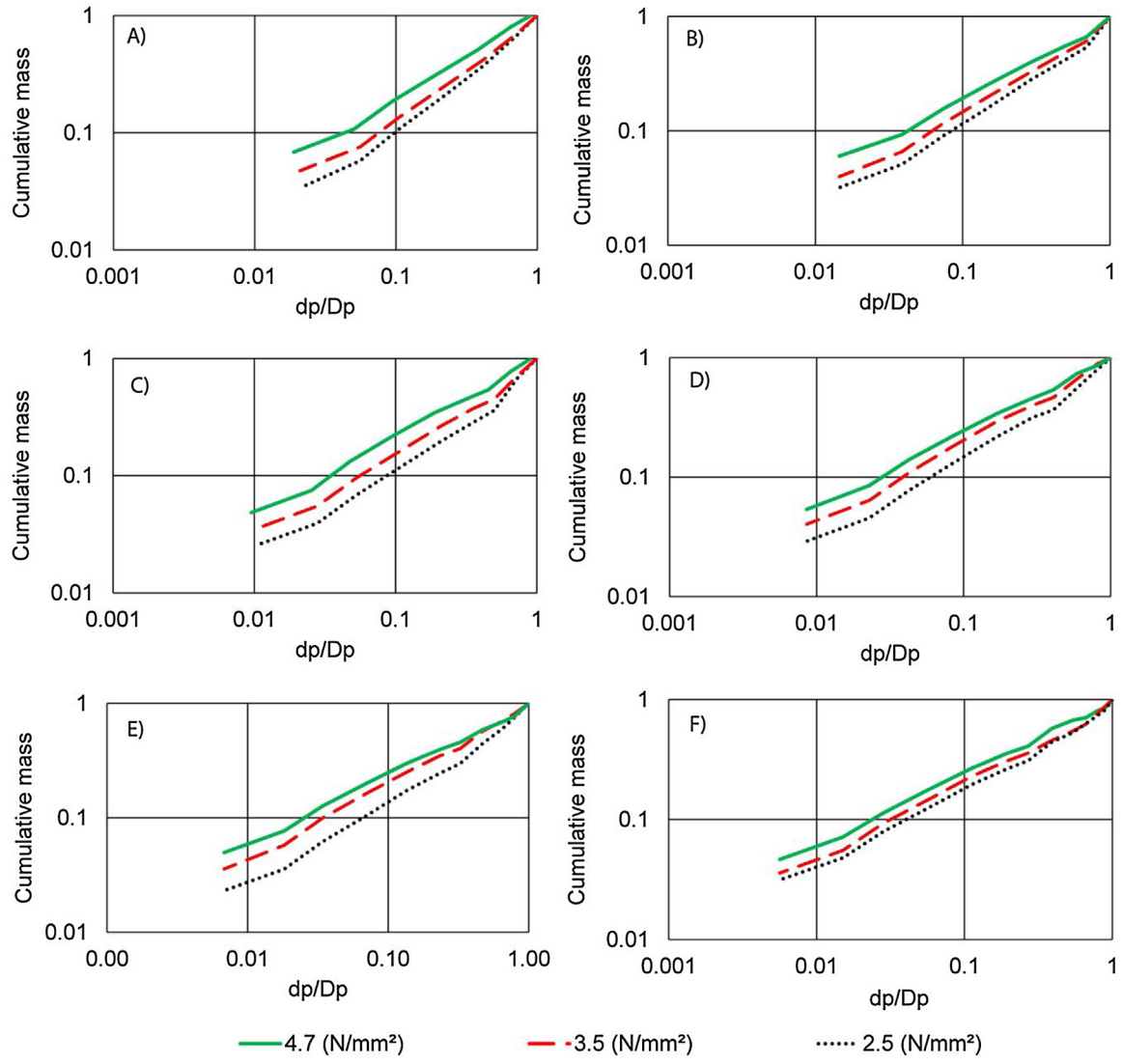

Fig. 5 – Results of the piston-die test at three specific pressure forces (Fsp), with different narrow ranges of particle sizes; A) −4 + 3.15 mm size range, B) −6.3 + 4 mm size range, C) −8 + 6.3 mm size range, D) −9.5 + 8 mm size range, E) −12.5 + 9.5 mm size range and F) −14 + 12.5 mm size range.

Table 4 – The parameter values were determined for different piston pressures. All parameters are dimensionless.

Fsp (N/mm²)	Function parameters	Fine particles (−8 + 3 mm)	Medium particles (−12.5 + 8 mm)	Coarse particles (−14 + 12.5 mm)
2.5	k	0.626	0.713	0.767
	n_1	0.731	0.708	0.629
	n2	2.355	3.200	3.717
3.5		Fines particles (−8 + 3 mm)	Medium particles (−14 + 8 mm)	–
	k	0.756	0.884	
	n_1	0.711	0.642	–
	n2	3.195	1.933	
4.7	k	0.915	0.962	
	n_1	0.677	0.608	–
	n2	1.596	1.396	
Single particle compression	k			0.282
	n_1	–	–	0.946
	n2			4.018

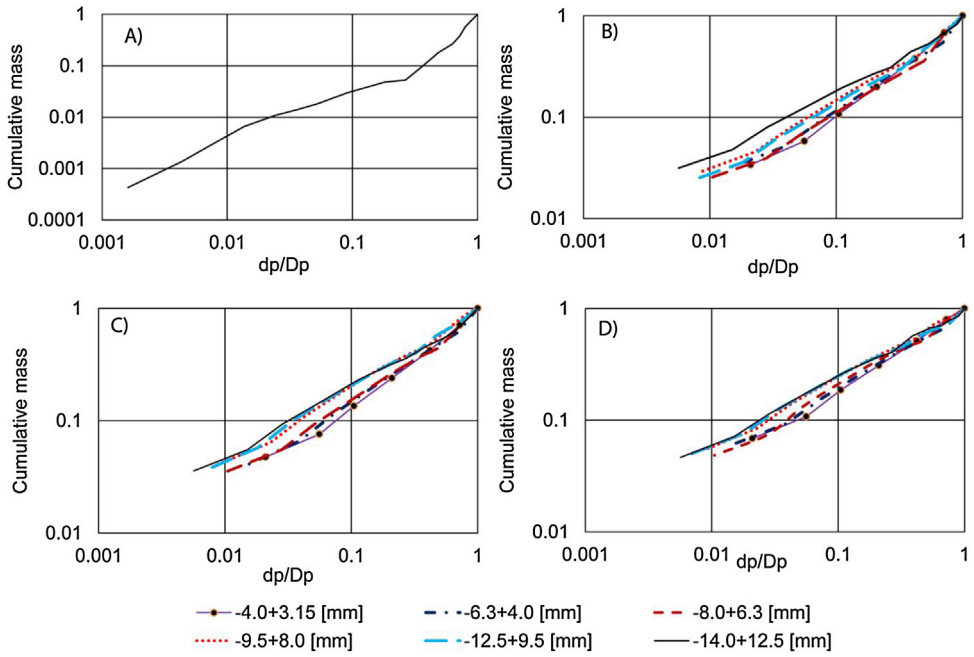

Fig. 6 – Results of the piston-die tests with different narrow particle sizes (mm) at three specific pressing forces (Fsp); A) single particle compression test at 2.5 [N/mm^2], B) bed compression test at 2.5 [N/mm^2], C) bed compression test at 3.5 [N/mm^2] and D) bed compression test at 4.7 [N/mm^2].

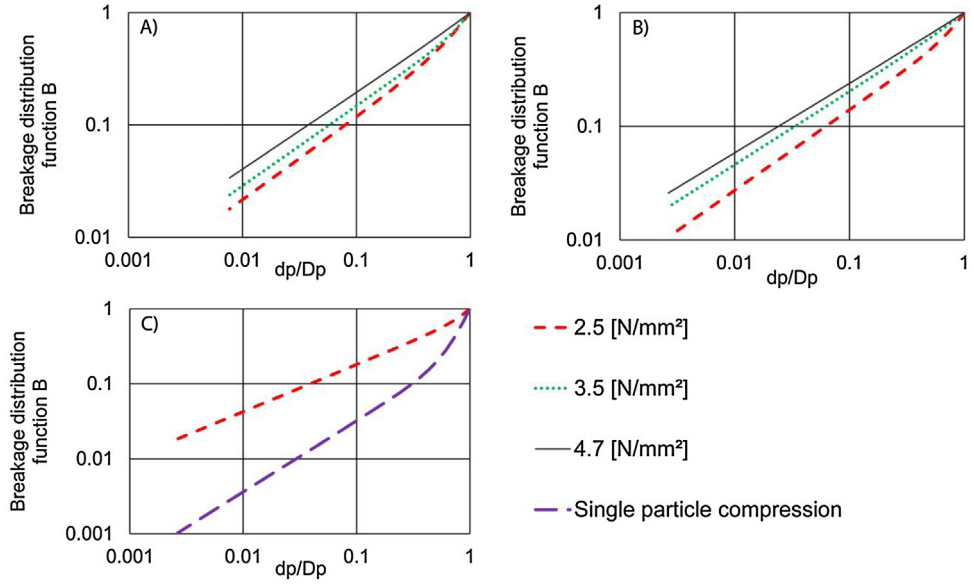

Fig. 7 – Breakage distribution function divided by particle size ranges and operative conditions; A) for particles ranged between 3.0–8.0 mm, B) for particles ranges between 8.0 mm and 12.5 mm, C) for particle size ranges between 12.5 mm and 14.0 mm.

As a result, the block scheme for the particle size distribution model predication shows a categorisation according to the particle range that will be submitted under single particle compression, and those that will be subjected to bed particle compression conditions. Furthermore, in the bed particle compression stage, the breakage function parameter values (taking into account the narrow size range) were also introduced into the calculation, using a selection function which discriminates the feed vector into the size ranges (Eq. 12).

$$C = \begin{cases} dp < 8 \\ 8 < dp < 12.5 \\ 12.5 < dp \end{cases} \quad (12)$$

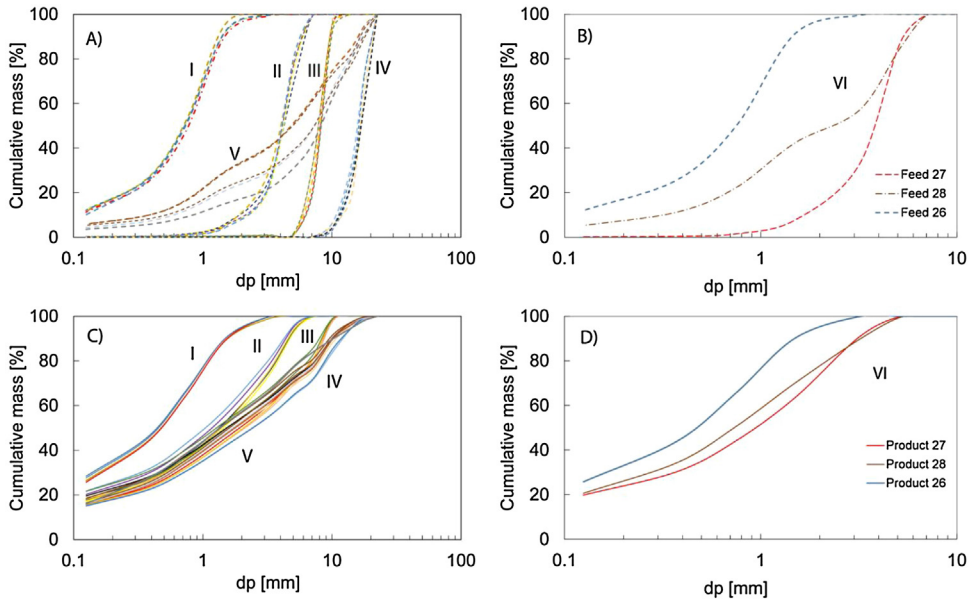

Fig. 8 – Sieve analysis on inputs and outputs of all tests performed in the HPGR. A) feed PSD re-grouped in the five categories from I to V, B) feed PSD curves of experiments 26 to 28, C) PSD product curves of all experiments from 1 to 25 categorised from group I to V, D) product PSD curves of experiments 26 to 28.

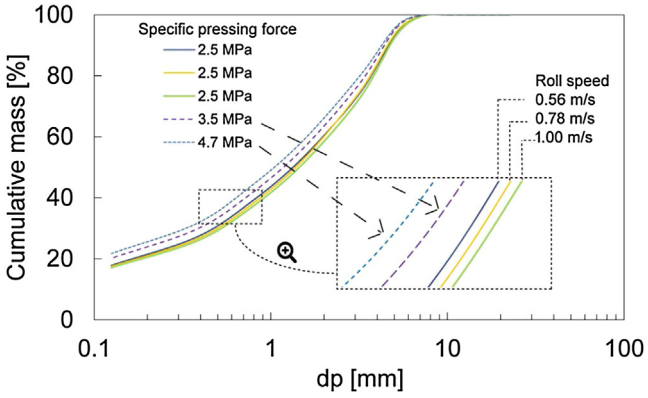

Fig. 9 – Analysis of the experiments from 6 to 10, zooming the product curves when varying the roll speed and the specific pressing force.

Thus, from the Eq. 12, the variable C could vary depending on the top feed particle size. In this case, they took the values 8 mm and 12.5 mm.

The model prediction and error calculation were computed, and the results show an average of 6.2 RMSE, 5.4 RMSE on the fine phases (particles under 750 microns), and 6.9 on the coarse phases (Table 5). The most remarkable fitted curves are presented in Fig. 10A, where tests 21 to 25 are shown. The overall error is around 2.06 RMSE, as in the case of the test 25 as an example, with differences in the fine phases reaching only 1.96 RMSE. The predictions of the product for test 16, 17, and 23 (Fig. 10B–D) are also acceptable, with less than 4.0 RMSE. The poorest results for model fitting were obtained from tests in category II and III (Fig. 11A). They represent tests for model calibration, and their model performance is not as relevant as the tests from the fifth category, as these, used a heterogeneous particle size distribution, which is what appears in real plants (Fig. 11B–D).

Table 5 – Root mean square error calculations of all tests simulations performed with the industrial HPGR (test 1–25) and lab-scale HPGR (test 26–28).

Category	Test	Overall	Coarse	Fines
	1	5.8	4.9	8.1
	2	3.3	2.8	5.2
I	3	2.7	2.6	3.8
	4	3.6	2.8	5.2
	5	5.9	3.0	9.4
	6	12.2	8.6	18.4
	7	11.5	7.0	17.2
II	8	10.7	5.7	16.3
	9	8.0	3.6	18.4
	10	9.1	4.3	13.2
	11	9.6	12.3	2.3
	12	11.6	14.8	3.2
III	13	10.2	13.0	2.9
	14	10.9	13.3	6.2
	15	13.4	15.1	11.8
	16	3.20	3.43	3.07
	17	3.03	2.51	4.47
IV	18	4.07	3.59	5.68
	19	4.38	5.31	1.24
	20	3.32	3.13	4.26
	21	2.21	1.91	3.14
	22	2.26	1.89	3.31
V	23	2.50	2.30	3.30
	24	2.48	1.88	3.92
	25	2.06	1.96	2.59
	26	2.18	2.30	1.98
VI	27	5.02	6.20	2.21
	28	7.20	1.84	12.55

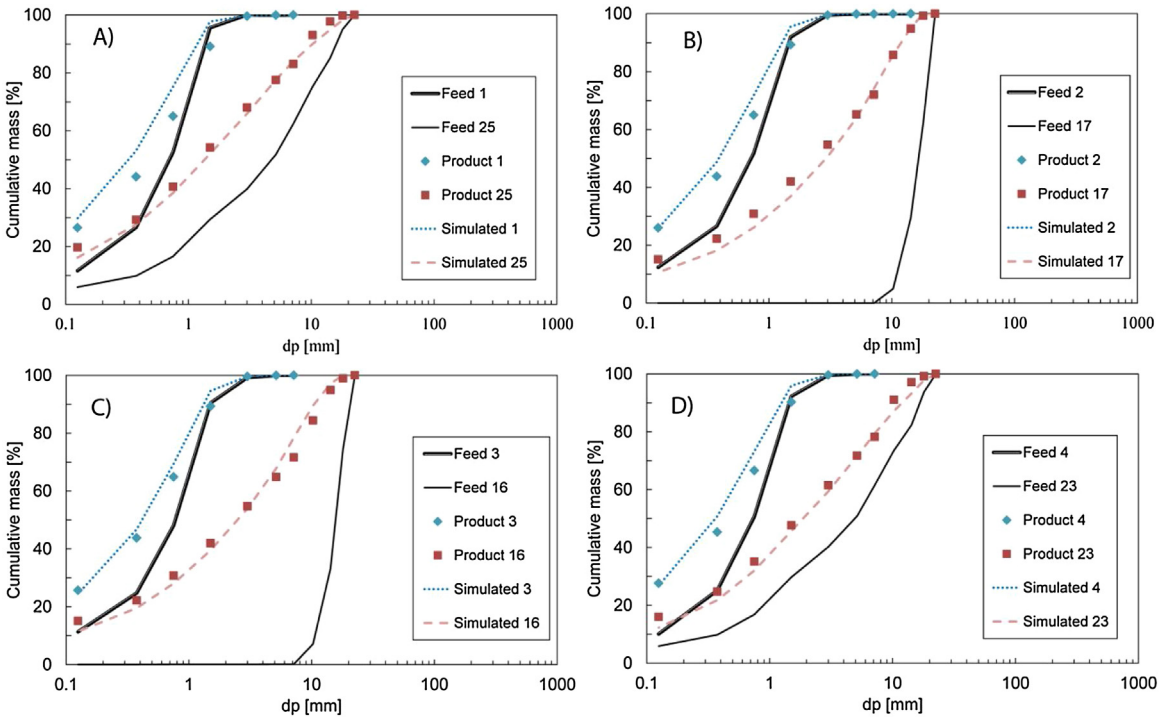

Fig. 10 – Feed, experimental, and simulated curves for different test with the industrial HPGR; A) test 1 and test 25, B) test 2 and 17, C) test 3 and 16, D) test 4 and 23.

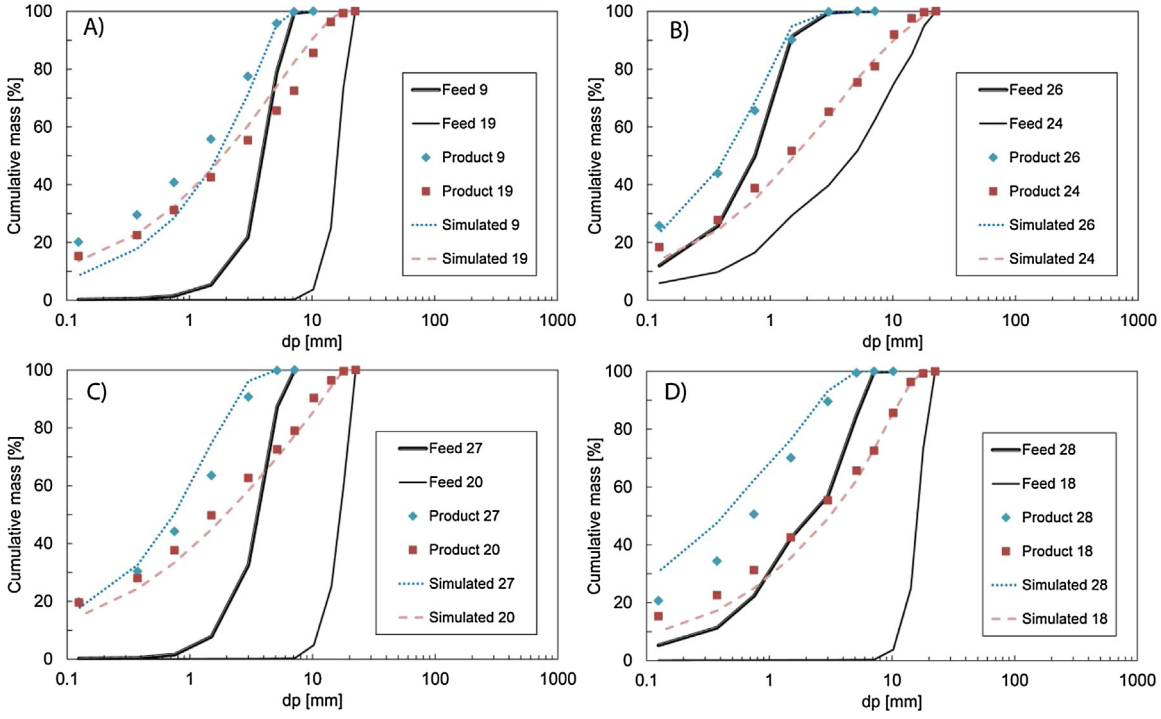

Fig. 11 – Feed, experimental and simulated curves for different test with industrial HPGR; A) Test 9 and test 19, B) Test 24 and 26, C) Test 20 and 27, D) Test 18 and 28.

3.3. *Parameters dependency on operative conditions*

The model for HPGR presented in Anticoi et al. [22] is complemented by the new findings in the present work, where the operative conditions of a specific pressing force were found to have an influence on the breakage distribution function parameters. This link can be observed in Fig. 12. The k parameter, which is defined as the main fine phase producer in a

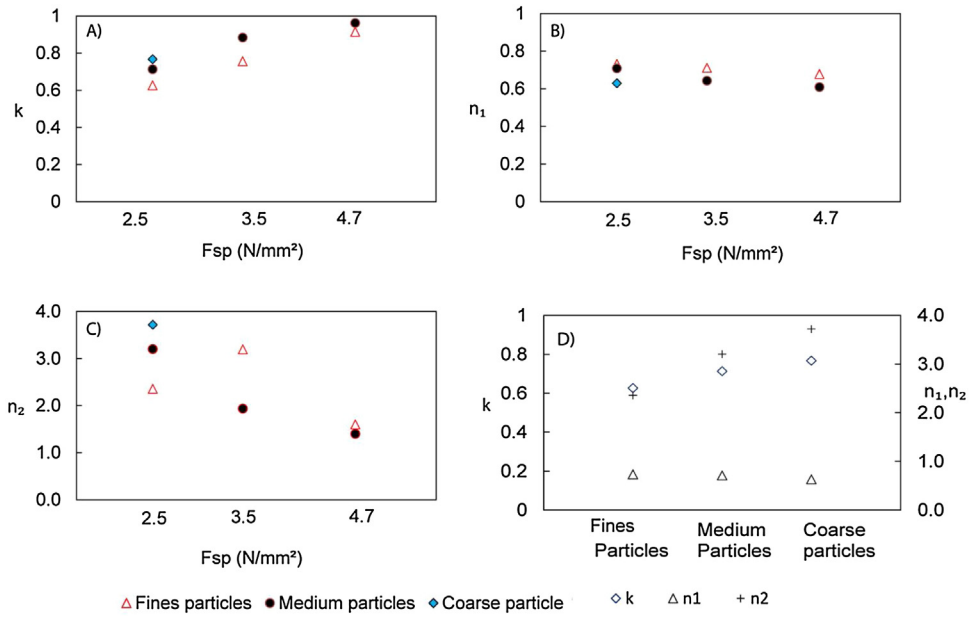

Fig. 12 – Relationship between the breakage function parameters and the specific pressing force. A) k parameters against Fsp, B) n_1 against Fsp, C) n_2 against Fsp and D) behaviour of all parameters and their size ranges under a specific pressing force of 2.5 [N/mm^2].

breakage event [16,19], increases with the specific pressure for all particle size ranges (Fig. 12A). The parameter n_1 is also responsible for the fine generation, but it has more influence on the quality of the slope of the curve generated by the distribution function [19]. The variation of the parameter n_1 is minimal, and it has no influence of the specific pressing force, as can be observed in Fig. 12B. Some studies define this parameter as material characteristic dependent [11,20].

In parallel, if the parameter k is related to the generation of fines, the form 1-k should refer to the generation of coarse particles, and so does the parameter n_2. This parameter varies with respect to the specific pressing force, and consequently, n_2 must be inversely proportional to the applied specific pressing force (Fig. 12C).

Regarding the relationships among the parameters and with the different mono-particle sizes determined in this paper, the parameters k and n_2 increase directly with the parent particle size at 2.5 N/mm^2 of specific pressing force. Meanwhile, the parameter n_1 remains constant for all particle size types (Fig. 12D).

The gap, defined as the minimum distance between the rolls during the grinding operation, is not static. The floating rolls create two types of gap: the zero-gap, which is the initial set up of the rollers, and the working gap, which is produced when the material passes through the mill rolls. The behaviour trend of this operative condition was also studied in order to determine its relationship with some other characteristic of the process or with the material itself. For the large HPGR type, the zero-gap is 10 cm. Fig. 13 shows the operational gap for all tests of groups I to V. The different values of the gap for the previously defined categories are easily observable. When the feed particle size increases, represented by the top-size parameter D_{80}, the operational gap also increases (Fig. 13A). However, at a certain cut-point, the trends are inversed: for the heterogeneous feed particle size distribution, the D_{80} decreases and the gap continues increasing.

There is an evident influence of the specific pressing force on the working gap (Fig. 13B), and it seems not to have much relation to the roll speed (Fig. 13C). The material moisture appears more dispersed when compared with the gap size (Fig. 13D).

The material porosity refers to the voids or spaces that exist between particles, and the cavities within each particle. The perceptible step in the size of the gap produced in the last category group may be related to the change in the porosity of the mill feed material (Fig. 13E). In the cases of relatively mono-size feed materials (from categories I to IV) the porosity remains constant. The heterogeneous distribution of particle sizes (category V) generates a filling of the cavities produced by the larger particles at the expense of the smaller particles, causing a decrease of the porosity. Thus, a more cohesive and competent material is formed, creating a resistance of the same material against compression, and therefore a greater opening of the working gap.

Comparing the characteristics against each other, more relations can be established. The working gap behaves in a way that is directly proportional to the feed particle size distribution, which is represented by the value D_{80}. The particle sizes of groups I to IV are slightly positively sloped (Fig. 14A) for all HPGR tests, except for group V, in which the gap size is considerable increased with respect to the rest of the values. As seen in Fig. 14A, in the tests with same specific pressing force but varying roll speed, in the plot against the feed size (Fig. 14B), no variations in the working gap are observed. However, some points from the V group are isolated from the others points. It seems that all tests with an increment of the porosity show

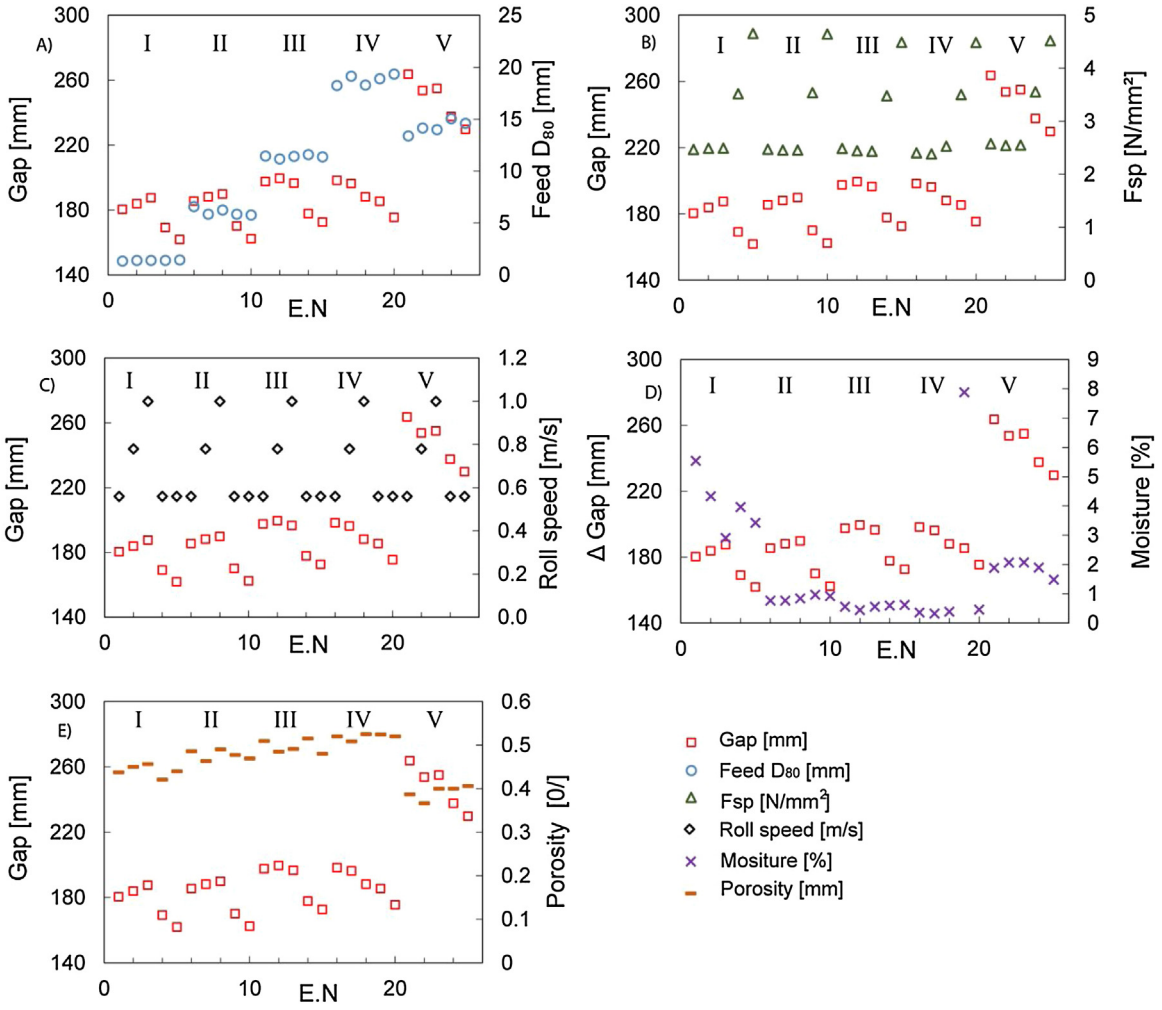

Fig. 13 – Graphics showing the relationship of the operational gap with other process characteristics. A) gap against feed D_{80}, B) gap against specific pressing force Fsp, C) gap against roll speed, D) gap against material moisture, and E) gap against material porosity.

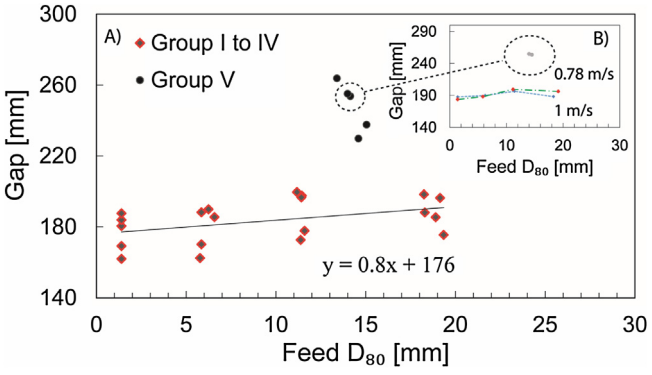

Fig. 14 – Plots of the trends discovered in the gap size and some process conditions, in this case, the top-feed size D_{80}. A) gap against feed D_{80} of al test, B) gap against feed D_{80} taking test with same pressure but varying roll speed.

low resistance of the floating roll to the material, leading to an increase of the working gap size.

Fig. 15 shows how the size of the working gap is influenced by the specific pressing force. The average slope value is 11.67, and 0.52 is the standard deviation between all curves; the trend is the same for all particle size classes when the tests are conducted with the same specific pressing force.

The porosity is another key parameter in the working gap overture. The porosity ranged from 0.36 to 0.41(differential values), representing the tests with a value of the working gap size that was over 220 mm (Fig. 16). It is also interesting to observe small variations in group V when the specific pressing force increases: the floating roll reacts to this, producing the gap size increment (from 225 mm to 250 mm), even when the porosity range between them is imperceptible (0.40–0.41).

Despite the dispersion of the material moisture shown in Fig. 13D, Fig. 17 indicates some tendencies of the working gap

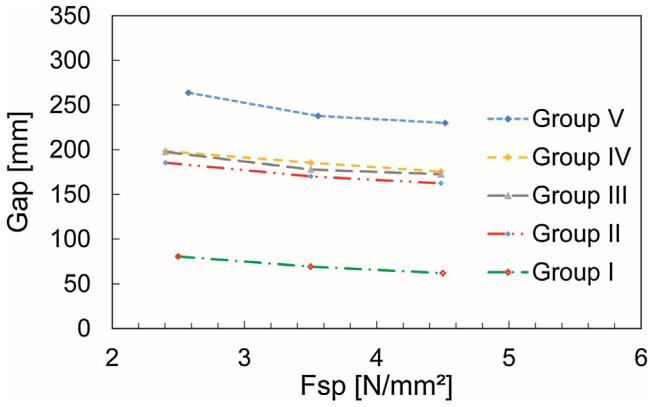

Fig. 15 – The working gap results are plotted against the specific pressing force, when the test are run with same roll speed.

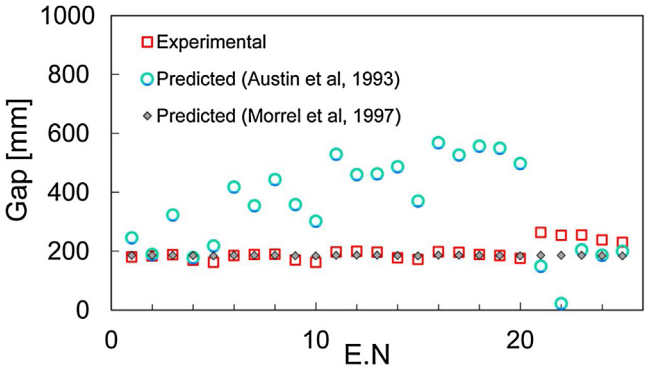

Fig. 18 – Working gap plots. The experimental data and predicted values from Austin et al. [6] are represented on the main axis. The predicted values by Morrel et al. [8] are presented on the secondary axis.

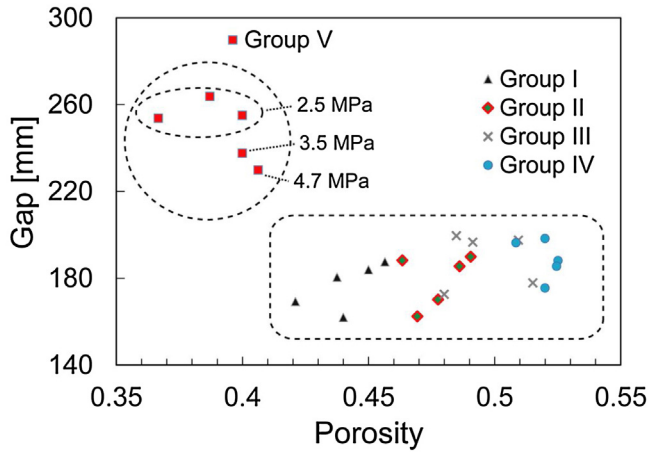

Fig. 16 – Working gap as affected by the material porosity. The dotted circles indicate tests from the same group and inside the tests with their specific pressing forces.

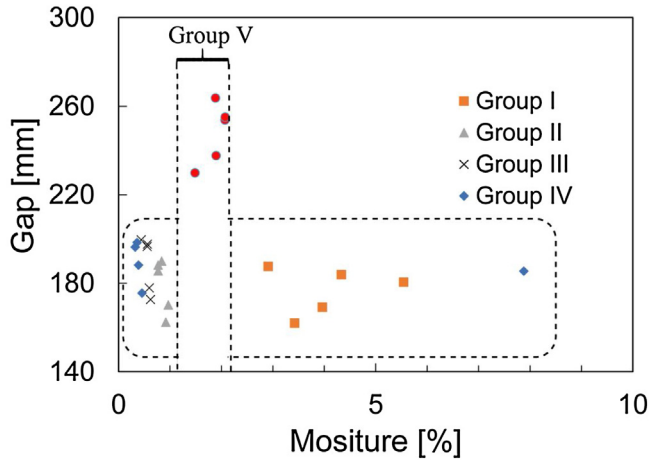

Fig. 17 – Working gap compared with material moisture.

size under a certain limited humidity range. It is possible that for some moisture values, the material resistance is stimulated to the point of compression, favouring the movement of the rollers, and then increasing the working gap size.

After these observations, a comparison with previous phenomenological models was undertaken, and they show some coincidences in the working gap determination (Fig. 17). However, it does not fit well in the high porosity zone (Fig. 18).

4. Conclusions

The model to predict the particle size distribution in a lab-scale HPGR was validated in an industrial device. The mathematical approach is based on various previously used mathematical approaches, one of which is the breakage distribution function. This function includes some parameters that are related to mineral characteristics, and also to the compression mechanism and operative conditions. In this case, the specific pressing force generates finer particles and the model interprets this condition, through the parameters k and n_2 of the breakage distribution function, with the parameter n_1 being the least affected. These model parameters are also sensible to the feed particle size and their values are also described in this paper. The comparison between simulated and experimental data when the model is run with a heterogeneous feed particle size material is remarkably good with the error reaching less than 3.0 RMSE.

The working gap is a process condition which also depends on the operative and material characteristics. When the specific pressing force increases, the gap is also influenced, showing a clear tendency to open the working gap overture. The influence of the speed of the rollers on the grinding process is slightly noticeable. Therefore, for this work, was not taken into account for the metallurgical model. The trends of the working gap when the nature of the material changed were probed, in this case, changes were to the feed top-size, moisture, and porosity.

Although in this work a single type of material is used, the model demonstrates its consistency due to its dependency in terms of the material characteristics and operative conditions

of the process, rather than using reverse back-calculations to determine the model parameters. This makes it a valuable tool for improving mineral processing, or in a flowsheet that includes this kind of device.

Conflicts of interest

The authors declare no conflicts of interest.

Acknowledgments

This work was supported by the European commission research and innovation programme Horizon 2020, through the project denominated OptimOre, grant number 642201. The authors would like to thank Technische Universität Bergakademie Freiberg and Prof. Dr.-Ing. Holger Lieberwirth for managing the tests with the HPGR Köppern manufacturer. This work was completed with the support of the company Köppern Aufbereitungstechnik GmbH & Co.KG (KAT), Freiberg, Germany. Thanks in particular to Dr. Felix Heinicke and Dr. Marcel Pfeifer for the help and the managing of the Köppern pilot plant in the Freiberg university facilities.

REFERENCES

[1] European Commission. Study on the review of the list of critical raw materials; 2017. Available online: https://publications.europa.eu/en/publication-detail/publication/08fdab5f-9766-11e7-b92d-01aa75ed71a1/language-en (accessed on 22 October 2018).
[2] Datta A, Rajamani RK. A direct approach of modeling batch grinding in ball mills using population balance principles and impact energy distribution. Int J Miner Process 2002;64:181–200.
[3] Fuerstenau DW, Abouzeid AZ. The energy efficiency of ball milling in comminution. Int J Miner Process 2002;67(4):161–85.
[4] Pérez-García EM, Bouchard J, Poulinc É. Integration of a liberation model in a simulation framework for comminution circuits. Miner Eng 2018;126:167–76.
[5] Abouzeid AZM, Fuerstenau DW. Grinding of mineral mixtures in high-pressure grinding rolls. Int J Miner Process 2009;93:59–65.
[6] Austin LG, Weller KR, Lim IL. Phenomenological modelling of the High pressure grinding rolls. In: Proceedings of the XVIII International Mineral Processing Congress. 1993. p. 87–95.
[7] Austin LG, Trubelja PM. The capacity and product size distribution of high pressure grinding rolls. In: Proceedings of the IV Meeting of the Southern Hemisphere of Mineral Technology. 1994. p. 49–67.
[8] Morrel S, Lim W, Tondo L. Modelling and scale up of the high pressure grinding rolls. In: In: Proceedings of the XX International Mineral Congress. 1997. p. 117–26.
[9] Daniel MJ, Morrell S. HPGR model verification and scale-up. Miner Eng 2004;17(11–12):1149–61.
[10] Torres M, Casali A. A novel approach for the modelling of high-pressure grinding rolls. Miner Eng 2009;22:1137–46.
[11] Kelly EG, Spottiswood DJ. The breakage function; what is it really? Miner Eng 1990;3(5):405–14.
[12] Kwon J, Jeong J, Cho H. Simulation and optimization of two-stage ball mill grinding circuit of molybdenum ore. Adv Powder Technol 2016;27:1073–85.
[13] Hill P, Ka M. Statistics of multiple particle breakage. Aiche J 1996;42–46:1600–11.
[14] Hasanzadeh V, Farzanegan A. Robust HPGR model calibration using genetic algorithms. Miner Eng 2011;24:424–32.
[15] Austin LG, Luckie PT. Methods for determination of breakage distribution parameters. Powder Technol 1972;5:215–22.
[16] Anticoi H, Guasch E, Hamid SA, Alfonso P, Oliva J, Bascompta M, et al. Mineral and mechanical characterization of tantalum and tungsten ores. Minerals 2018;8(4):170.
[17] Austin LG, Luckie PT. The estimation of Non-normalized breakage distribution parameters from batch ginding test. Powder Technol 1971:267–71.
[18] Klimpel RR, Austin LG. The back-calculation of specific rates of breakage and non-normalized breakage distribution parameters from batch grinding data. Int J Miner Process 1977;4:7–32.
[19] King RP. Modelling and simulation of mineral processing systems. Butterworth: Heinemann, Oxford; 2001.
[20] Chimwani N, Glasser D, Hildebrandt D, Metzger JM, Mulenga FK. Determination of the milling parameters of a platinum group minerals ore to optimize product size distribution for flotation purposes. Miner Eng 2013;43-44:67–78.
[21] Tavares LM. Particle weakening in high-pressure roll grinding. Miner Eng 2005;18:651–7.
[22] Anticoi H, Guasch E, Hamid SA, Oliva J, Alfonso P, Bascompta M, et al. An improved high pressure roll crusher model for tungsten and tantalum ores. Minerals 2018;8(11):483.
[23] Delaney GW, Cleary PW, Morrison RD, Cummins S, Loveday B. Predicting breakage and the evolution of rock size and shape distributions in AG and SAG mills using DEM. Miner Eng 2013;50-51:132–9.
[24] Schönert K, Sander U. Shear stresses and material slip in high pressure roller mills. Podwer Technol 2002;122:136–44.
[25] Ghorbani Y, Mainza AN, Petersen J, Becker M, Franzidis JP, Kalala JT. Investigation of particles with high crack density produced by HPGR and its effect on the redistribution of the particle size fraction in heaps. Miner Eng 2013;43-44:44–51.
[26] Alfonso P, Castro D, Garcia-Valles M, Tarragó M, Tomasa O, Martinez S. Recycling of tailings from the Barruecopardo tungsten deposit for the production of glass. J Therm Anal Calorim 2016;125(2):681–7.
[27] Whiten WJ, Walter GW, White ME. A breakage function suitable for crusher models. In: Proceedings of the IV Tewkesbury Symposium. 1979. p. 19.1–3.